sought to be patented and the prior art are such that the subject matter as a whole would have been obvious at the time the invention was made to a person having ordinary skill in the art to which said subject matter pertains. Patentability shall not be negatived by the manner in which the invention was made."
6. *Chakrabarty* v. *Diamond*, 206 *U.S. Pat. Q.* 193 (U.S. Supreme Court, 1980).
7. A. Diepenbrock, C. Neagley, D. Jeffrey, *Am. Pat. Law Assoc. Sel. Leg. Pap.* 1 (No. 2), 81 (1983).
8. *American Patent Law Association Plant Variety Protection Committee Annual Report* (1981).
9. 19 *U.S. Code*, sects. 1337 and 1337a.
10. 35 *U.S. Code*, sect. 271.
11. 7 *U.S. Code*, sect. 2541.
12. *In re Argoudelis*, 168 *U.S. Pat. Q.* 99 (Court of Customs and Patent Appeals).
13. 7 *U.S. Code*, sect. 2401(a).
14. 7 *U.S. Code*, sect. 2402.
15. 7 *U.S. Code*, sect. 2401(a)(1).
16. 7 *U.S. Code*, sect. 2401(a)(2).
17. *In re Waller* (U.S. Secretary of Agriculture decision, 14 July 1981).
18. 7 *U.S. Code*, sect. 2401(a)(3).
19. 7 *U.S. Code*, sect. 2544.
20. 7 *U.S. Code*, sect. 2543.
21. *Delta and Pine Land Co.* v. *Peoples Gin Co.*, 694 *Fed. Rep.* 2nd ser. (Fifth Circuit Court, 1983).
22. 28 *U.S. Code*, sect. 1498.
23. U.S. House of Representatives, *House Rep. No. 1129* (71st Congress, Second Session, 10 April 1930; U.S. Senate, *Senate Rep. No. 315* (71st Congress, Second Session, 3 April 1930).
24. *Graver Tank & Mfg. Co.* v. *Linde Air Products Co.*, 339 *U.S. Rep.* 605 (U.S. Supreme Court, 1950).
25. *Ex parte Jackson*, 217 *U.S. Pat. Q.* 204 (Patent and Trademark Office Board of Appeals, 1982).
26. *Regnum Veg.* **22**, 30 (1961).

**RESEARCH ARTICLE**

# A Deep 6-Centimeter Radio Source Survey

E. B. Fomalont, K. I. Kellermann
J. V. Wall, D. Weistrop

Abstract. *The Very Large Array has been used to survey a small region of sky at a wavelength of 6 centimeters down to a completeness level of 60 microjanskys—about 100 times weaker than the faintest radio sources that have been detected with other instruments. The observed source count at flux densities below 100 millijanskys converges in a manner similar to the lower frequency counts, although there is some evidence for an excess of sources weaker than 100 microjanskys. The sources in the survey are preferentially identified with faint galaxies.*

The shortest wavelength at which extensive radio source surveys have been made is 6 cm. At this wavelength surveys by the National Radio Astronomy Observatory (NRAO) and Max-Planck-Institut (MPI) have covered most of the northern sky down to a limiting flux density of 600 millijanskys (mJy), while the various Parkes surveys provide complete samples of sources down to 1 Jy (*1*). Over limited regions of the sky other single-dish surveys made at NRAO and MPI are complete to 35 mJy (*2*), 20 mJy (*3*), 15 mJy (*4*), and 14 mJy (*5*). Synthesis surveys covering even smaller regions have reached levels of 4.5 mJy at Westerbork (*6*) and 0.5 mJy at the Very Large Array (VLA) (*7*). We have used the VLA to extend the surveys to sources that are as faint as 60 μJy at 6 cm, or about 100 times weaker than levels reached with other instruments at any wavelength. Source catalogs constructed from these surveys provide the basis for further studies in the radio region and in other parts of the spectrum. Further investigation is in progress on the nature of these weak radio sources, their spatial distribution and luminosity function, and how these properties change with cosmological epoch.

Counts of radio sources made at centimeter wavelengths are of particular interest since, for the stronger sources selected at this wavelength, flat-spectrum compact sources and steep-spectrum extended sources (which dominate the long-wavelength counts) are present in roughly equal numbers (*5, 8–10*). Previous surveys made at 6 cm for relatively bright sources show that for $S > 100$ mJy (approximately the 20,000 brightest sources in the sky) the counts are closely represented by the "Euclidean" law

$$\eta_0(S) = 90\ S^{-2.5} \qquad (1)$$

where $\eta_0(S)$ is the number of sources with flux density $S$ per unit flux density interval.

Between 10 and 100 mJy the 6-cm counts begin to decrease in a manner qualitatively similar to the long-wavelength counts of the steep-spectrum sources (*5, 8, 9*). However, the extended Euclidean plateau at 6 cm differs dramatically from the long-wavelength count, which is characterized by a steep rise for strong sources (the brightest 1000 or so) followed by a rapid decrease in the density of the weaker sources.

In this article we report on observations of very weak radio sources at 6 cm, and we discuss the angular size, spectra, and optical identification of these weak sources.

## Observations and Reductions

In order to investigate the number density of very faint radio sources, we have mapped a small area of sky, using the VLA to detect all sources with a flux density greater than 60 μJy. These new observations include the weakest radio sources yet cataloged and reach a source density of $6 \times 10^5$ sources per steradian. Supplemental information concerning this sample of sources was obtained through (i) VLA observations at 20 cm to determine the spectral index of the sources and (ii) optical observations with the 4-m telescope at Kitt Peak National Observatory (KPNO) to aid in the identification of the sources.

The 6-cm observations were made in the D configuration of the VLA to synthesize a 700-m-diameter antenna on a field centered at right ascension ($\alpha$) = $00^h15^m24^s$ and declination ($\delta$) = 15°33′00″ (epoch 1950.0). The resolution is about 18 arc sec and no emission will be missing for sources less than 120 arc sec in size. The general area of the field

E. B. Fomalont is a system scientist at the National Radio Astronomy Observatory, Socorro, New Mexico 87801. K. I. Kellermann is a senior scientist at the National Radio Astronomy Observatory, Green Bank, West Virginia 24944. J. V. Wall is head of Astrophysics and Astrometry Division at the Royal Greenwich Observatory, Herstmonceux Castle, Hailsham, East Sussex BN27 1RP, United Kingdom. D. Weistrop is a scientist at the Laboratory for Astronomy and Solar Physics, NASA-Goddard Space Flight Center, Greenbelt, Maryland 20771, and is a visiting astronomer at Kitt Peak National Observatory.

was not selected at random but was chosen for the following reasons. In order to observe during the night with the available scheduled time in the D configuration, the right ascension of the field had to lie near $1^h$. Several deep optical plates were available for the chosen field (selected area 68.1). A high-resolution x-ray map from the Einstein satellite covered most of the area near the field. Finally, observations at Westerbork at 20 cm showed that there were no bright sources near the field which would interfere with the VLA high-sensitivity radio survey (*11*). The specific location of the Deep Field was random within the area constrained by these criteria. These selection biases should not affect the statistics of the present survey.

The observing program was also designed to measure the fluctuations of the cosmic background radiation as well as the number density of weak sources. The results on the background fluctuations are given by Fomalont *et al.* (*12*). The observations consisted of four 12-hour periods on 27, 28, and 29 September and 2 October 1981 to give a total integration time of about 40 hours on one field. All observations were made at elevations greater than 14° above the horizon. The diameter of the field was limited by the primary beam size of the 25-m antennas: 8.9 arc min full width at half-maximum and 17.1 arc min full width to the first nulls. Both the phase tracking (fringe-stopping) and antenna pointing were located at the field center position. In addition, we observed ten other fields surrounding the Deep Field for about 40 minutes integration each in order to provide better statistics for the source count level above 350 μJy. We refer to these as the Intermediate Fields; the locations of the fields are given in Table 1.

Table 1. Field centers.

| Field | Position (epoch 1950.0) | |
|---|---|---|
| | α | δ |
| I1 | $00^h14^m25^s.84$ | 15°19′00″ |
| I2 | 00 15 24.00 | 15 19 00 |
| I3 | 00 13 27.63 | 15 33 00 |
| I4 | 00 14 25.84 | 15 33 00 |
| I5 | 00 16 22.16 | 15 33 00 |
| I6 | 00 13 27.63 | 15 47 00 |
| I7 | 00 14 25.84 | 15 47 00 |
| I8 | 00 15 24.00 | 15 47 00 |
| I9 | 00 14 25.84 | 16 01 00 |
| I10 | 00 15 24.00 | 16 01 00 |
| Deep | 00 15 24.00 | 15 33 00 |

The observations were made at night to avoid interference from the sun in the sidelobes of the antennas. The system noise temperature was 60 K in both left- and right-circular polarization channels, each with a bandwidth of 50 MHz. The antenna pointing was accurate to 0.3 arc min and the delay was tracked to better than 1.5 nsec. All data in which one antenna shadowed another were excluded from the analysis. The instrumental and atmospheric gain and phase fluctuations were monitored by observing the nearby calibrator source 0007 + 171 for 2 minutes at 30-minute intervals. The assumed position for the calibrator is $\alpha = 00^h07^m59^s.383$, $\delta = 17°07'37''.50$ (epoch 1950.0). An observation of 3C48, with an assumed flux density of 5.36 Jy at 4.9 GHz, was used to determine the flux density scale of the observations. It should not be in error by more than 3 percent.

Radio maps were made by following standard Fourier inversion techniques and the clean algorithm was used to remove the effects of the sidelobes in the synthesized beam pattern. The data were mapped so that each 20-second sample of the visibility data at each baseline was given equal weight (so-called natural weighting) to produce the optimum signal-to-noise ratio for a point source. The area of the cleaned synthesized region was 25.6 arc min square (256 by 256 map with a pixel separation of 6 arc sec), which extends beyond the null of the primary beam pattern of the 25-m antennas. The resolution of the map was 18 arc sec. For each of the 4 days of observations radio maps of the field were made separately in the right- and left-circular polarizations. These maps were compared to judge the reliability and sensitivity of the observations. The total intensity map was made by averaging the eight maps (4 days times two polarizations).

The sensitivity parameters of the observations are given in Table 2. The detection level was 60 μJy for a point source. Over most of the field of view the root-mean-square (rms) noise was 11 μJy; however, the noise level increased up to 18 μJy within the inner 5 percent of the field. The increased noise near the field center was caused by low-level correlated signals between the antennas; details are given by Fomalont *et al.* (*12*). Seven percent of the data were edited in order to decrease the effect of these signals. For the Intermediate Fields the detection level of 350 μJy was about 4.5 times the rms noise level.

The 20-cm VLA observations were obtained in February 1983 in the C configuration, which nearly matched the resolution of the 6-cm observations. Seven hours were integrated on the Deep Field, and four other surrounding fields were each observed for 25 minutes in order to overlap all of the intermediate 6-cm fields. Table 2 also contains the sensitivity parameters for these observations. The data were used to obtain estimates of the flux density at 20 cm for the sources found in the 6-cm observations; hence no detection limit is applicable. These data were reduced and processed in a manner similar to the 6-cm data.

Optical observations with the prime focus RCA/CCD camera on the 4-m Mayall telescope at KPNO were made on two nights in November 1982. Eight CCD frames, each 3 by 5 arc min in area, were needed to cover all the sources in the Deep Field. No observations were

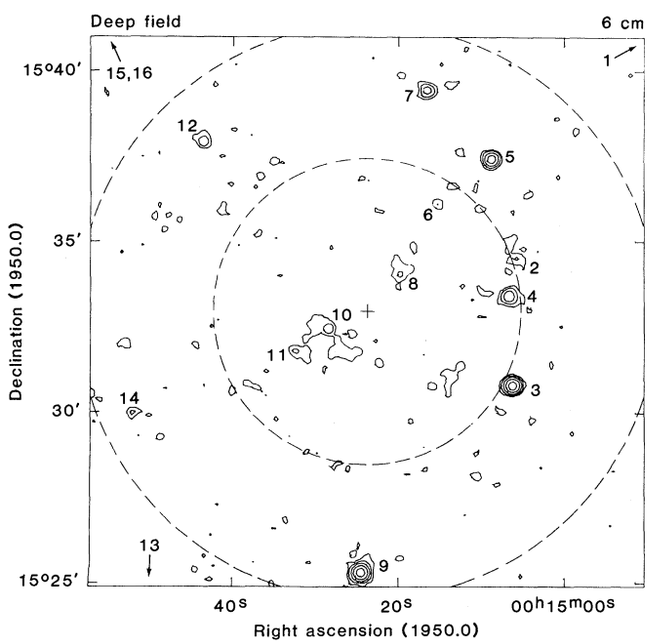


Fig. 1. Contour map of the Deep Field at 6 cm. Contour levels are at 25, 50, 100, 200, and 400 μJy per beam. Only sources with a second contour level have been included in Table 3 and are labeled with their catalog numbers. The cross shows the position of the field center and the two dashed circles show the 50 percent and 8 percent sensitivity loci of the primary beam. Sources 1, 13, 15, and 16 lie outside the 8 percent response. No correction for the primary beam response has been applied to the map.

made for the sources in the Intermediate Fields. A complete discussion of the CCD observations, analysis, and results will follow (*13*). Preliminary analysis shows that 11 of the 13 sources in Table 3 have certain or probable identifications, based on coincidence of the radio and optical positions to about 1.5 arc sec. From the surface density of galaxies at magnitude $V = 25^m$, this criterion leads to a 2 percent chance of misidentification (*14*).

For sources in the Intermediate Fields, identifications were made solely from the Palomar Sky Survey (PSS) prints. An identification was made on the basis of a radio-optical coincidence to less than about 4 arc sec. Only 6 of the 35 sources were identified and the probability of misidentification is less than 1 percent. The identification type and magnitude are listed in columns 8 and 9 of Table 4.

Table 2. Observational sensitivities.

| Field | Wavelength (cm) | Integration time (min) | Detection limit* (mJy) | Root-mean-square noise* (mJy) | Comments |
|---|---|---|---|---|---|
| Deep | 6 | 2378 | 0.060 | 0.011† | 27 antennas—7 percent data deleted |
| Intermediate | 6 | 39 | 0.350 | 0.068 | 27 antennas |
| Deep | 20 | 475 | | 0.030 | 26 antennas |
| Intermediate | 20 | 25 | | 0.150 | 26 antennas |

*Uncorrected for primary beam attenuation. †0.018 at field center.

### The 6-Centimeter Source Count

The radio map of the Deep Field at 6 cm is shown in Fig. 1. The region displayed covers 16.0 arc min square, and the primary beam response circles for half-power and 8 percent power are shown. Sixteen sources with a peak map flux density above 50 μJy were found and are listed in Table 3. The flux densities in Table 3 have been corrected for primary beam attenuation. The sources are designated by numbers in order of their right ascension. Nine sources are included in the complete sample above 60 μJy. This limit is 4.5 times the rms noise level within 2 arc min of the field center and 5.5 times the rms noise outside this region. There is less than a 4 percent chance that any source in the complete sample is fictitious. Four sources lie outside the 8 percent primary beam contour; hence, a flux density cannot be determined. Those with an asterisk and a listed flux density have a peak flux density on the map between 50 and 60 μJy. Because of the dearth of sources and their small average angular size, it is unlikely that several of the sample sources are, in fact, components of one source. In addition, all but two of the nine sources are identified with individual optical features.

The parameters for each source were obtained by fitting the map intensities to an elliptical-Gaussian-shaped model. For sources which appeared to be resolved, the integrated map flux density was also estimated by summing the map intensities around the source. Because there were some variations in the background level in the map, a zero level was also determined for many of the sources before fitting them with a Gaussian. The map flux density was then converted into a true flux density by using the primary beam response of the VLA 25-m antennas at 6 cm. This correction is known to an accuracy of 2 percent or better out to a radius of 7.7 arc min, which corresponds to a response of 8 percent of the on-axis response. No correction for bandwidth smearing was necessary.

The same analysis was performed on the ten Intermediate Fields and the source parameters are given in Table 4. Only sources with a peak map flux density greater than 350 μJy, within the 8 percent power response of the map, are in the complete sample. This detection level is 5.5 times the rms noise. When a source appeared on more than one map, the source parameters were averaged. The uncertainty in source position and flux density was estimated from the scatter between the determinations as well as from the individual fits. The agreement between the multiple observations was consistent with the individual errors.

By analyzing the number distribution of map intensities, it is possible to estimate the source density below 100 μJy. This so-called $P(D)$ analysis was performed on the Deep Field by the method outlined by Wall *et al.* (*15*). The analysis took into consideration the increase of noise in the map near the center.

The number density of sources at 6 cm for the complete sample was calculated by the method of Katgert *et al.* (*16*). The search area associated with each source was equal to the area over which the source would have been detected over the 60- or 350-μJy limit for the Deep Field or the Intermediate Field, respectively, or the area within the 8 percent primary beam response, whichever was smaller. The number density derived from this analysis is shown in Table 5.

A small correction to the count was made to compensate for sources with a peak flux density less than 60 μJy in the Deep Field or 350 μJy in the Intermediate Field but with an integrated flux density greater than these limits. We estimated this correction from the measured average ratio of the integrated to

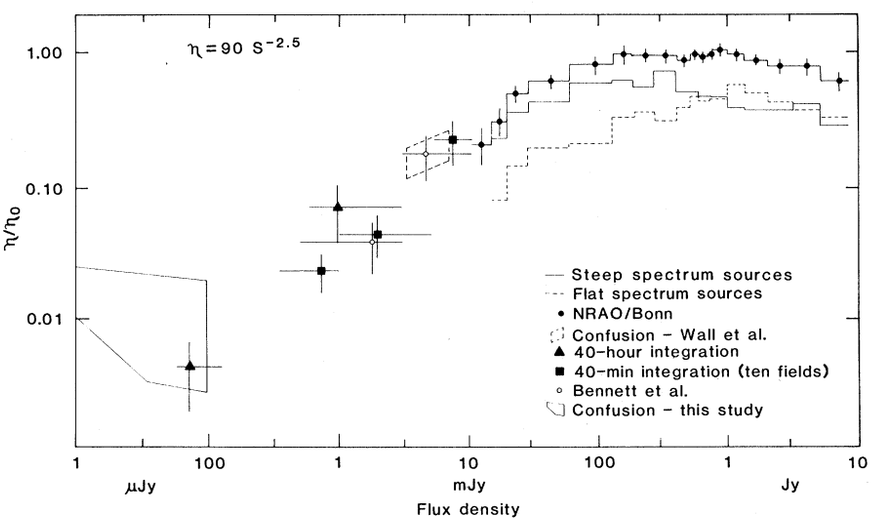


Fig. 2. Number count of sources at 6 cm. The count has been normalized to the Euclidean differential count of 90 $S^{-2.5}$. Subcounts for the steep spectrum (thin solid line) and flat spectrum (thin dashed line) are also shown. References for the higher flux density data points are given in the text.

the peak flux density, which was 1.14 in this survey. As an independent check, the correction to the count was also obtained as follows: (i) the distribution of largest angular size (LAS) in the range 20 to 33 μJy was taken from Downes (*17*), (ii) a source brightness model was taken as a rectangle with dimensions LAS by LAS/4, and (iii) the number count of sources less than 60 μJy was assumed to have a differential count of 500 $S^{-1.75}$. This model also produces about the same ratio of integrated to peak flux density as was observed.

Correction for the angular size of the

Table 3. Deep Field source list.

| Deep Field number (1) | Position (epoch 1950.0) α (2) | Position (epoch 1950.0) δ (3) | Flux density (mJy) 6 cm (4) | Flux density (mJy) 20 cm (5) | Spectral index (6) | Angular size Arc sec × arc sec (7) | Angular size Degree |
|---|---|---|---|---|---|---|---|
| 1* | $00^h14^m44^s.86 \pm 0^s.05$ | 15°42′29″.5 ± 1″.0 | | | | <10 | |
| 2 | 00 15 06.00 0.30 | 15 34 28.0 5.0 | 0.52 ± 0.04 | 1.20 ± 0.20 | −0.70 ± 0.18 | 80 × 30 | 10 |
| 3 | 00 15 06.22 0.03 | 15 30 48.0 0.3 | 1.49 0.04 | 2.70 0.20 | −0.50 0.08 | <6 | |
| 4 | 00 15 06.66 0.04 | 15 33 24.1 0.5 | 0.360 0.027 | 0.18 0.05 | +0.58 0.29 | <9 | |
| 5 | 00 15 08.81 0.03 | 15 37 24.8 0.4 | 1.14 0.07 | 1.10 0.10 | +0.03 0.11 | <9 | |
| 6* | 00 15 15.23 0.10 | 15 36 07.4 1.0 | 0.083 0.015 | 0.07 0.03 | +0.14 0.47 | <15 | |
| 7 | 00 15 16.59 0.03 | 15 39 26.5 0.4 | 0.77 0.08 | 1.80 0.20 | −0.71 0.15 | <9 | |
| 8* | 00 15 19.10 0.20 | 15 34 05.0 4.0 | 0.184 0.026 | 0.26 0.05 | −0.29 0.24 | 50 | |
| 9 | 00 15 24.54 0.03 | 15 25 19.3 0.3 | 7.86 0.24 | 19.20 0.50 | −0.75 0.04 | <6 | |
| 10 | 00 15 28.53 0.10 | 15 32 26.7 2.0 | 0.070 0.016 | 0.13 0.05 | −0.52 0.45 | <12 | |
| 11 | 00 15 32.45 0.20 | 15 31 48.6 2.0 | 0.072 0.015 | 0.22 0.06 | −0.94 0.34 | <15 | |
| 12 | 00 15 43.59 0.05 | 15 37 57.3 1.0 | 0.78 0.07 | 1.10 0.10 | −0.29 0.13 | 20 × 10 | 50 |
| 13* | 00 15 48.97 0.07 | 15 23 39.3 1.5 | | | | <15 | |
| 14* | 00 15 52.02 0.07 | 15 29 58.5 0.6 | 0.51 0.12 | 0.60 0.10 | −0.14 0.29 | <20 | |
| 15* | 00 16 01.80 0.06 | 15 41 50.1 0.7 | | | | <9 | |
| 16* | 00 16 06.14 0.06 | 15 45 26.3 2.0 | | | | 25 × 12 | 107 |

*Not in complete sample

Table 4. Intermediate Field source list.

| Intermediate Field number (1) | Position (epoch 1950.0) α (2) | Position (epoch 1950.0) δ (3) | Flux density (mJy) 6 cm (4) | Flux density (mJy) 20 cm (5) | Spectral index (6) | Angular size Arc sec × arc sec (7) | Angular size Degree | Identification Type (8) | Identification Magnitude (9) |
|---|---|---|---|---|---|---|---|---|---|
| 1* | $00^h12^m39^s.58 \pm 0^s.20$ | 15°53′02″.3 ± 2.0 | | | | <20 | | g† | 19 |
| 2* | 00 12 44.10 0.10 | 15 56 19.9 1.0 | | | | 25 × 10 | 61 | | |
| 3 | 00 13 16.57 0.10 | 15 48 42.0 0.7 | 6.81 ± 0.55 | 15.7 ± 1.6 | −0.70 ± 0.13 | 36 × 10 | 98 | Sp | 16 |
| 4 | 00 13 21.05 0.11 | 15 46 26.4 1.5 | 0.62 0.06 | 0.8 0.2 | −0.21 0.27 | <15 | | | |
| 5 | 00 13 23.86 0.03 | 15 34 39.8 0.4 | 1.76 0.09 | 4.8 0.5 | −0.84 0.12 | <10 | | | |
| 6 | 00 13 26.82 0.11 | 15 49 02.8 1.2 | 0.73 0.06 | <0.8 | >−0.08 | <15 | | | |
| 7 | 00 13 28.72 0.12 | 15 34 01.7 0.6 | 0.66 0.07 | 1.2 0.3 | −0.50 0.27 | <12 | | | |
| 8 | 00 13 40.09 0.03 | 15 34 40.7 0.4 | 2.25 0.14 | 5.1 0.7 | −0.69 0.15 | <10 | | | |
| 9* | 00 13 58.39 0.10 | 15 31 01.7 1.3 | 3.73 0.35 | 9.0 0.5 | −0.74 0.11 | <15 | | | |
| 10* | 00 14 02.94 0.13 | 15 39 53.8 2.0 | | | | <20 | | | |
| 11 | 00 14 06.11 0.04 | 15 51 53.0 0.3 | 19.44 1.77 | 54.0 2.0 | −0.86 0.10 | <12 | | g | 19 |
| 12 | 00 14 15.40 0.20 | 15 31 50.3 1.2 | 0.62 0.06 | 1.4 0.3 | −0.68 0.24 | <12 | | | |
| 13 | 00 14 16.60 0.15 | 15 19 20.0 0.8 | 0.93 0.05 | 1.1 0.2 | −0.14 0.19 | <12 | | | |
| 14 | 00 14 19.75 0.10 | 15 30 29.8 0.6 | 1.78 0.13 | 8.7 0.6 | −1.33 0.10 | <10 | | | |
| 15 | 00 14 22.53 0.15 | 15 16 52.8 1.5 | 0.64 0.10 | <0.8 | >−0.20 | 20 | | | |
| 16* | 00 14 25.96 0.50 | 15 34 24.4 2.0 | 0.34 0.04 | <0.5 | >−0.32 | <15 | | g | 20 |
| 17 | 00 14 26.20 0.07 | 15 22 52.9 0.4 | 1.38 0.08 | 4.3 0.3 | −0.95 0.09 | <12 | | | |
| 18 | 00 14 28.42 0.08 | 15 54 01.0 2.0 | 2.33 0.15 | 4.4 0.4 | −0.53 0.11 | <15 | | | |
| 19 | 00 14 29.20 0.15 | 15 26 39.2 1.5 | 7.05 0.91 | 8.6 0.8 | −0.17 0.16 | 50 × 20 | 10 | | |
| 20* | 00 14 38.10 0.15 | 15 50 03.0 2.0 | 0.58 0.06 | 0.8 0.3 | −0.27 0.39 | <15 | | | |
| 21* | 00 14 44.00 0.25 | 16 00 32.3 2.2 | | | | <15 | | | |
| 22 | 00 14 44.75 0.10 | 15 42 31.0 1.5 | 5.96 0.46 | 18.5 1.0 | −0.95 0.09 | <10 | | | |
| 23 | 00 15 14.48 0.05 | 15 23 06.2 1.0 | 1.42 0.10 | 2.6 0.3 | −0.51 0.14 | <12 | | | |
| 24 | 00 15 20.46 0.06 | 15 45 03.8 1.0 | 0.83 0.06 | 2.0 0.3 | −0.74 0.17 | <12 | | | |
| 25 | 00 15 24.52 0.04 | 15 25 18.1 0.6 | 8.05 0.28 | 21.4 1.0 | −0.82 0.06 | <10 | | | |
| 26* | 00 15 25.40 0.50 | 15 59 47.0 4.0 | | | | 40 × 15 | 53 | | |
| 27 | 00 15 30.10 0.06 | 15 56 15.7 0.6 | 2.14 0.22 | 5.5 0.6 | −0.79 0.15 | <15 | | g | 20 |
| 28 | 00 15 33.69 0.07 | 15 46 47.0 2.0 | 0.96 0.08 | 2.4 0.4 | −0.77 0.19 | <12 | | | |
| 29 | 00 15 41.80 0.40 | 15 57 15.0 15.0 | 9.70 1.76 | 15.0 5.0 | −0.37 0.38 | 60 × 30 | 30 | | |
| 30 | 00 15 48.99 0.05 | 15 23 39.4 0.3 | 11.66 0.78 | 4.3 0.3 | +0.84 0.10 | <12 | | | |
| 31* | 00 15 56.15 0.10 | 16 04 04.1 0.6 | | | | <10 | | | |
| 32 | 00 16 02.50 0.15 | 15 32 28.0 1.4 | 0.80 0.10 | 4.3 0.5 | −1.41 0.17 | <15 | | | |
| 33* | 00 16 24.94 0.20 | 15 37 16.2 2.5 | | | | 35 | | | |
| 34 | 00 16 34.95 0.07 | 15 35 42.0 0.4 | 5.71 0.34 | 10.8 1.1 | −0.54 0.12 | <10 | | | |
| 35 | 00 16 39.20 0.20 | 15 39 17.2 1.1 | 4.85 0.78 | 4.5 0.4 | +0.06 0.18 | <15 | | g | 19 |

*Not in complete sample. †Types: g, faint galaxy; Sp, spiral galaxy; blank, no identification.

Table 5. Source densities at 6 cm.

| Flux density range (mJy) | Average flux density (mJy) | Area of sky ($10^{-5}$ sr$^{-1}$) | Number* | | | $\eta_c/\eta_0$ | Comments |
|---|---|---|---|---|---|---|---|
| | | | $\eta$ | $\eta_c$ | $\eta_0$ | | |
| 0.01–0.10 | | | | | | 0.010 ± 0.004 | *P*(*D*) analysis |
| 0.06–0.60 | 0.122 | 0.728 | 4 | 5.5 | 910 | 0.0060 ± 0.0030 | From Deep Field |
| 0.60–3.00 | 0.967 | 1.568 | 4 | 4.2 | 58 | 0.072 ± 0.036 | From Deep Field |
| >3.00 | 7.865 | 1.568 | 1 | 1.0 | 5.7 | 0.174 | From Deep Field |
| 0.35–1.00 | 0.733 | 5.86 | 9 | 10.0 | 426 | 0.023 ± 0.008 | From Intermediate Fields |
| 1.00–5.00 | 1.952 | 10.87 | 8 | 8.6 | 188 | 0.046 ± 0.016 | From Intermediate Fields |
| >5.00 | 8.706 | 15.68 | 8 | 8.1 | 26.6 | 0.305 ± 0.107 | From Intermediate Fields |

*$\eta$, Number observed in flux density range; $\eta_c$, number observed after correction for average source angular size; $\eta_0$, number expected from Euclidean model.

sources in the *P*(*D*) analysis is somewhat uncertain. We applied the integrated/peak flux density ratio of 1.14 ± 0.07 (estimated error) as a multiplicative factor in the density of sources derived from the *P*(*D*) analysis.

The resultant source count at 6 cm and those at higher flux densities are shown in Fig. 2. The count has been normalized to a differential Euclidean count of $\eta_0 = 90\ S^{-2.5}$. The enclosed area in Fig. 2 between 10 and 100 μJy shows the range in the count derived from the *P*(*D*) analysis.

The new 6-cm data show that in the range 0.1 mJy $< S <$ 100 mJy the source count decreases and can be represented by the differential law $\eta = 500\ S^{-1.75}$. Between 10 μJy and 100 μJy the *P*(*D*) analysis indicates a somewhat flatter count, but the accuracy of the slope in this range is limited by the excess low-level fluctuations near the center of the field, where the observations are most sensitive to weak sources. The observed flattening may represent the contribution may represent the contribution of a faint new population—that is, normal galaxies—but further observations will be required to confirm this. It is clear from the *P*(*D*) data, however, that the count does not drop even more steeply below 100 μJy. Our results are thus compatible with the flattening of the count reported at 20 cm (*18, 19*).

## Spectral Index and Identification of the Sample Sources

The map of the Deep Field at 20 cm is shown in Fig. 3. All the sources listed in Table 3 have some counterpart in the 20-cm map. Many sources at 20 cm were detected on both the Deep Field and one or more of the four other fields. The source parameters were suitably averaged after fitting with a Gaussian component. The agreement between the 20-cm and 6-cm positions and angular sizes was within the expected errors. For the several sources where the quality of the 20-cm position or angular size estimate was as good as that at 6 cm, the results in Table 3 contain the appropriate average. For extended sources the same regions in the 6- and 20-cm maps were integrated to obtain the respective flux densities.

The spectral indices α, where $S = \nu^{\alpha}$, for the sources in the Deep Field and Intermediate Field are given in column 6 of Tables 3 and 4. The value and error were derived from the measured flux density and error at 20 and 6 cm. Spectral indices more negative than −0.5 are generally referred to as normal or steep-spectrum and are typically associated with galaxies or other extended sources. So-called flat-spectrum sources ($\alpha > -0.5$) result from self-absorption in compact sources such as quasars (*8*). The separate source subcounts for these two classes of radio sources reflect their different space density, luminosity function, and spatial evolution.

Figure 2 shows the subcounts for flat- and steep-spectrum sources constructed from source count and spectral index data given elsewhere (*1, 2, 6, 8, 20*). The count for the flat-spectrum population begins to converge near 1 Jy, whereas the steep-spectrum population only converges below about 100 mJy and the separate peaks in the two subcounts combine to give the apparent Euclidean slope observed for the overall count over a wide range in flux density. Our data from the Deep Field and Intermediate Field surveys contain too few sources for us to make a meaningful separation in each flux density bin, but the measured fractions of flat- and steep-spectrum sources found indicate that the weak source count for both classes converges roughly as $S^{-1.75}$.

For the 29 sources in the Intermediate Field survey above 350 μJy completeness level, 13 (45 percent) have flat spectra and 16 (55 percent) have steep spectra, while for the Deep Survey sources, 7 (64 percent) have flat spectra and only 4 (36 percent) have steep spectra. This represents a marginally significant increase in the fraction of flat-spectrum sources over the value of 25 percent for

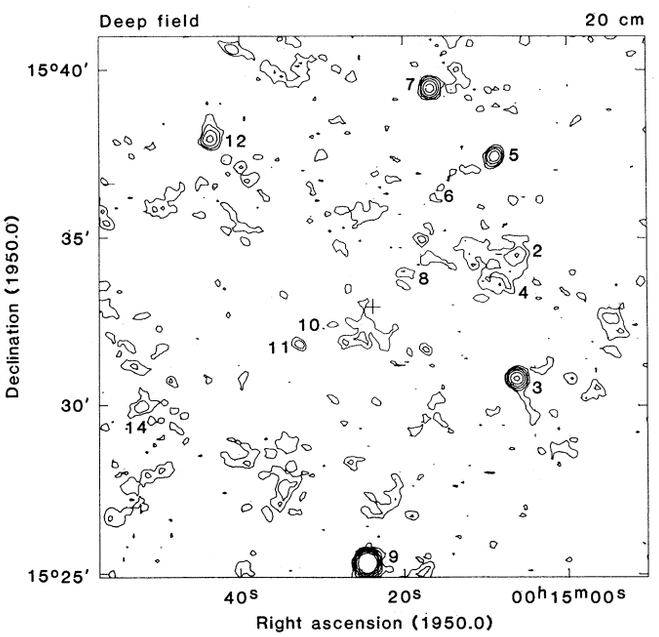


Fig. 3. Contour map of the Deep Field at 20 cm. Contour levels are at 62.5, 125, 250, 500, 1000, and 2000 μJy flux units per beam. Sources labeled in the 6-cm map of Fig. 1 have been labeled in this map. The cross shows the position of the field center. No correction for the primary beam response has been applied to the map.

sources above 50 mJy (*2, 8, 21*). This increase in the fraction of very weak flat-spectrum sources may reflect the new source population discussed above for the total source count below 100 μJy. It is beyond the scope of this article to discuss in detail models of the radio source population, but analyses of the type reported by Peacock and Gull (*10*) can give further information on the space distribution, luminosity function, evolution, and redshift cutoff of these weak radio sources.

The identification rate for the Intermediate Field sources, 4 in 25 in the complete sample, is comparable to that found by others who used the PSS for identifications at the level of 1 to 10 mJy. All but one of the objects are fainter than $18^m$ on the red print of the PSS and are probably distant galaxies. Source IF3 is identified with a $16^m$ spiral galaxy.

The CCD observations at the Deep Field source positions reach $V \simeq 25^m$. Our preliminary analysis indicates that of the nine sources in the complete sample, five have reliable identification, two have probable identification, and two are unidentified. Certainly, no galactic objects, stars, supernova remnants, or planetary nebulae are present in the sample. Many of the images are extended and are presumably galaxies: the modest seeing (2 arc sec full width at half-maximum) and 0.6 arc sec pixel size generally do not allow the morphological type to be distinguished. The source DF2 has an extremely low surface brightness and is about 5 arc sec in size. This object has the largest radio image of all of the Deep Field sources, 80 by 30 arc sec. It could be a single galaxy or a tight and distant cluster of galaxies. Finally, it is interesting to note that the two brightest sources in the complete sample are the two sources that are not identified. This is consistent with the majority of the Deep Field sources representing emergence of a low-luminosity population, differing from the brighter 6-cm sources, which are basically radio-luminous objects undergoing strong cosmic evolution.

Approximately 15 percent of the sources in the Deep Field and Intermediate Field have an angular extent >20 arc sec, about the same percentage as for sources over 100 times as bright. This is consistent with the average angular size of radio sources being only a weak function of flux density below about 100 mJy (*17, 22*).

## Conclusion

The observed density of radio sources near 100 μJy at 6 cm shows that the count decreases rapidly below a flux density of 100 mJy, but that it again flattens in slope below 100 μJy. This suggests that the weaker radio sources are relatively nearby low-luminosity objects, in contrast to the high-luminosity sources which are characteristic of samples above 100 mJy. Source spectra of the weakest sources appear to be flatter than those of sources that are about 100 times brighter, and the optical counterparts of these sources are preferentially faint galaxies in groups.

### References and Notes


1. I. I. K. Pauliny-Toth, A. Witzel, E. Preuss, H. Kuhr, K. I. Kellermann, E. B. Fomalont, M. M. Davis, *Astron. J.* **83**, 451 (1978).
2. F. N. Owen, J. J. Condon, J. E. Ledden, *ibid.* **88**, 1 (1983).
3. J. Maslowsky, I. I. K. Pauliny-Toth, A. Witzel, H. Kuhr, *Astron. Astrophys.* **95**, 285 (1981).
4. J. E. Ledden, J. J. Broderick, J. J. Condon, R. L. Brown, *Astron. J.* **85**, 780 (1980).
5. I. I. K. Pauliny-Toth, A. Witzel, E. Preuss, J. A. Baldwin, R. E. Hills, *Astron. Astrophys. Suppl.* **34**, 253 (1978).
6. A. G. Willis and G. K. Miley, *Astron. Astrophys.* **76**, 65 (1979).
7. C. L. Bennett, C. R. Lawrence, J. A. Garcia-Barreto, J. N. Hewitt, B. F. Burke, *Nature (London)* **301**, 686 (1983).
8. K. I. Kellermann, *Phys. Scr.* **21**, 664 (1980).
9. J. V. Wall and C. R. Benn, in *Galactic and Extragalactic Radio Sources*, D. S. Heeschen and C. M. Wade, Eds. (Reidel, Dordrecht, Netherlands, 1982), pp. 441–449.
10. J. Peacock and S. F. Gull, *Mon. Not. R. Astron. Soc.* **196**, 64 (1981).
11. R. A. Windhorst, thesis, Leiden University (1984).
12. E. B. Fomalont, K. I. Kellermann, J. V. Wall, *Astrophys. J. Lett.* **277**, L23 (1984).
13. D. Weistrop, J. V. Wall, E. B. Fomalont, K. I. Kellermann, in preparation.
14. R. G. Kron, *Astrophys. J. Suppl.* **43**, 305 (1980).
15. J. V. Wall, P. A. G. Scheuer, I. I. K. Pauliny-Toth, A. Witzel, *Mon. Not. R. Astron. Soc.* **198**, 221 (1982).
16. P. Katgert, J. K. Katgert-Merkelijn, R. S. Le Poole, H. van der Laan, *Astron. Astrophys.* **23**, 171 (1973).
17. A. Downes, in *Galactic and Extragalactic Radio Sources*, D. S. Heeschen and C. M. Wade, Eds. (Reidel, Dordrecht, Netherlands, 1982), pp. 393–400.
18. H. van der Laan, P. Katgert, R. Windhorst, M. Oort, *Proc. Int. Astron. Union Symp. 104*, in press.
19. J. J. Condon and K. J. Mitchell, *Astron. J.*, in press.
20. A. Witzel, J. Schmidt, I. I. K. Pauliny-Toth, V. Nauber, *ibid.* **84**, 942 (1980).
21. J. J. Condon and J. E. Ledden, *ibid.* **86**, 643 (1981).
22. R. D. Ekers and G. K. Miley, in *Radio Astronomy and Cosmology*, D. Jauncey, Ed. (Reidel, Dordrecht, Netherlands, 1977), pp. 109–117.
23. The National Radio Astronomy Observatory is operated by Associated Universities, Inc., under contract with the National Science Foundation. Kitt Peak National Observatory is operated by the Association of Universities for Research in Astronomy, Inc., under contract with the National Science Foundation.